

pubs.acs.org/JPCB Article

Chelated Magnesium Logic Gate Regulates Riboswitch Pseudoknot Formation

Raju Sarkar, Akhilesh Jaiswar, Scott P Hennelly, José N Onuchic,* Karissa Y Sanbonmatsu,* and Susmita Roy*



Cite This: J. Phys. Chem. B 2021, 125, 6479-6490



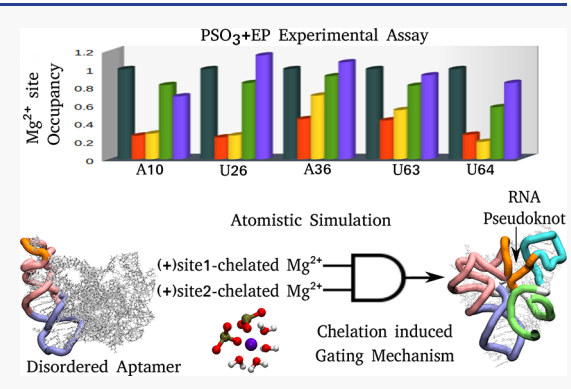
ACCESS

Metrics & More

Article Recommendations

Supporting Information

ABSTRACT: Magnesium plays a critical role in the structure, dynamics, and function of RNA. The precise microscopic effect of chelated magnesium on RNA structure is yet to be explored. Magnesium is known to act through its diffuse cloud around RNA, through the outer sphere (water-mediated), inner sphere, and often chelated ion-mediated interactions. A mechanism is proposed for the role of experimentally discovered site-specific chelated magnesium ions on the conformational dynamics of SAM-I riboswitch aptamers in bacteria. This mechanism is observed with atomistic simulations performed in a physiological mixed salt environment at a high temperature. The simulations were validated with phosphorothioate interference mapping experiments that help to identify crucial inner-sphere Mg²⁺ sites prescribing an appropriate initial distribution of inner- and outer-sphere magnesium ions to maintain a physiological ion concentration of monovalent and



divalent salts. A concerted role of two chelated magnesium ions is newly discovered since the presence of both supports the formation of the pseudoknot. This constitutes a logical AND gate. The absence of any of these magnesium ions instigates the dissociation of long-range pseudoknot interaction exposing the inner core of the RNA. A base triple is the epicenter of the magnesium chelation effect. It allosterically controls RNA pseudoknot by bolstering the direct effect of magnesium chelation in protecting the functional fold of RNA to control ON and OFF transcription switching.

■ INTRODUCTION

RNA folding into stable secondary and tertiary structures is the most important phenomenon for specific gene expression. RNA consists of a series of negatively charged phosphate groups in its phosphodiester backbone, but it still folds into a well-shaped compact structure overcoming the huge electrostatic repulsion. The presence of positively charged metal ions, hence, is crucial not only for charge neutralization, but they also coherently décor the ion atmosphere of RNA, in such a way, that RNA gets its optimal ambiance to fold and function.²⁻⁹ Among different prevalent metal ions in cellular composition, magnesium is eventually unique in stabilizing the compact fold of RNA.^{3,10} It creates a more effective ion atmosphere by directly interacting with the negatively charged phosphate group of the RNA backbone. However, physiologically, RNA hovers in a mixed-salt environment where it interacts with both monovalent potassium (K⁺) and divalent magnesium (Mg^{2+}) ions. $^{13-15}$

In solution, Mg²⁺ forms a hexa-hydrated complex with six water molecules surrounding in an octahedral manner, in the first solvation layer, ^{16,17} while the ion atmosphere of RNA involves three kinds of Mg²⁺ ions: (i) the diffuse ions, which are dynamic in nature, (ii) the outer-sphere ions, which interact with RNA but are separated from the RNA by a single

hydration layer, and (iii) the inner sphere ions, which directly interact with the phosphate groups of RNA.4,14,18 Although this classification is done based on the characteristics of Mg²⁺ ions, it is valid for monovalent K+ as well. 19 In general, it is hypothesized in many theoretical studies that an essential contribution to the stabilization of the native structure RNA comes from the diffuse ions. 20-23 For the inner-sphere ions to make direct contact with the phosphate groups of RNA, it is essential for them to partially dehydrate. 3,24 The partial dehydration of a hexa-hydrated Mg2+ complex to come into the direct contact of phosphate groups of RNA is energetically less favorable due to huge entropy loss.3 This explanation is also augmented by the slow exchange rate of a water molecule in the first solvation layer of Mg²⁺ (in the order of microseconds).²⁵ While all these explanations support the hypothesis that the stability of RNA structure is mostly contributed by the outer-sphere ions compared to an inner-

 Received:
 March 18, 2021

 Revised:
 May 25, 2021

 Published:
 June 9, 2021





sphere ion interaction, it is rather recently that a special type of inner-sphere ion coordination has been found to interact directly with a number of phosphate groups, thus supporting the inner core of the RNA fold. These inner-sphere ions that hold more than one phosphate group together are called *chelated* ions. Also, for chelated ions, it might be true that they generate electrostatic stress due to loss of entropy, but we cannot rule out the fact that the strong electrostatic interactions with multiple phosphate groups of RNA may outcompete the entropy loss, turning it into a favorable interaction. This demands a thorough calculation characterizing the free energy of chelation accounting for a real RNA system that is immersed in a solution of monovalent and divalent ion mixture mimicking the physiological functional ion environment for RNA. Although this is computationally highly challenging, our research in this direction is underway.

To unravel the microscopic picture of the ion-chelation effect on RNA structure, the slow exchange rate between Mg²⁺ and water appears as the bottleneck that narrows the revenue of characterization of the ion atmosphere with different computational approaches. Even a long-extended simulation often falls short to accurately probe such slow exchange dynamics with the aid of available empirical force fields relevant for biomolecular simulations. In one of our previous studies, we have performed ten 2 µs simulations of riboswitch S-adenosylmethionine-1 (SAM-1) in explicit water, using the salt buffer as potassium chloride and magnesium ions.³⁰ The simulation revealed slow RNA fluctuations with increasing magnesium concentrations. We found the strong association of outer-sphere magnesium ions with RNA that is mostly responsible to restrict the RNA dynamics.^{3,30} The slowness is also reflected in our estimated diffusion coefficient, which is in the range of 10 $\mu m^2/s$. In these early studies, we found that the biomolecular force fields, such as AMBER and CHARMM27, work well for a nucleic acid system with other small ions.^{31–36} However, understanding ion-binding properties and solvation free energy are different with Mg²⁺. Several attempts were made to study the correct structural, dynamic, and thermodynamic properties of the ion atmosphere of RNA. 25,34,35 In 2012, Villa and co-workers introduced some new parameters and validated them with the available experimental results to deal with such slow kinetics.²

Because of this slow timescale issue and a high degree of flexibility in the RNA structure, most of the models of RNA are limited to describe its ion atmosphere filled with only nonspecific diffused ions, at a low salt concentration range. Debye—Hückel electrostatics and nonlinear Poisson Boltzmann are used to treat the ionic environment as a continuum.^{37–40} In these approaches, molecular details such as ion—ion correlations and the discrete effects of the ions are generally ignored. To account for the ion—ion correlation, recently we have developed a generalized Manning counter-ion condensation model.^{41–43} This model additionally accounts for the irregular structure of RNA at physiological ionic concentrations, but the effects of inner-sphere ions were neglected.

The effect of site-specific Mg²⁺ is thought to be the most critical for the function of many RNA systems, including riboswitches, which is a key gene-regulatory RNA component abundantly found in bacteria.⁵ In recent times, many such chelation sites are being identified in the X-ray crystal structure of other RNA systems^{26–28} but their precise role in RNA fold stabilization has not been explored. In the crystallographic

study of 58-nucleotide ribosomal RNA, one chelated K^+ and one chelated Mg^{2+} are found. A,44,45 In hammerhead and glmS ribozymes, chelated Mg^{2+} was found to exert greater impact in their folding and catalysis. In the *Thermotoga petrophila* fluoride riboswitch, the fluoride ion is found encapsulated by three chelated Mg^{2+} ions, regulating gene expression through the transcription termination mechanism.

In our early wet-lab experiments, we found three innersphere Mg²⁺sites that are profoundly impactful for the stability of the SAM-I riboswitch. These are considered as hotspots for RNA stability. Two of these Mg²⁺ chelated sites are consistent with the crystal structure of Batey and co-workers.9 While our early structured-based model study shows that the presence of outer-sphere Mg²⁺ ions can induce open-to-closed transitions for the SAM-I riboswitch, 47 it is not known whether these transitions result from the implicit effect of site-specifically bound, chelated Mg^{2+} ions or independently from the dense outer-sphere cloud of Mg2+ surrounding the RNA. In this work, we will use the SAM-I riboswitch aptamer as a bestcharacterized RNA model to initiate the first study of chelated-Mg²⁺-RNA interactions in a mixed salt environment by performing extensive atomistic simulations combining knowledge from our phosphorothioate interference mapping experiments (Figure 1).

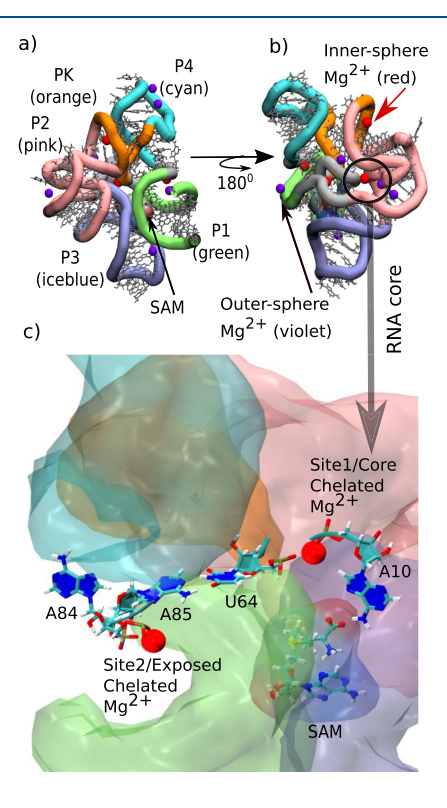


Figure 1. Equilibrium structure of SAM-I aptamer RNA along with its interactive Mg^{2+} ion environment. The snapshot is extracted from one of the equilibrium trajectories of SAM-I generated maintaining 300 K temperature, $\sim \! 100$ mM KCl, $\sim \! 2.0$ mM bulk Mg^{2+} concentration. (a) SAM-I with all helices. (b) 180^0 reorientation of (a). Inner (red) and outer-sphere (violet) Mg^{2+} ions are indicated in (b). The inner Mg^{2+} binding sites are consistent with our phosphorothioate interference experimental results. (c) Two chelated Mg^{2+} ions are identified: (i) one in the RNA core, close to the SAM ligand-binding site. The core chelated magnesium is indicated as site1- Mg^{2+} coordinating A10 and U64. (ii) Exposed chelated magnesium coordinating A84 and A85. The exposed chelated magnesium is referred to as site2- Mg^{2+} .

METHODS

RNA System. The SAM-I aptamer is a well-deserved RNA candidate to study the impact of Mg2+ chelation on RNA structure due to the following reasons: (i) as it is the first discovered riboswitch, its structural information at least at the aptamer level is well characterized compared to other RNA systems; (ii) existence of two chelated Mg2+ ions that are intricately associated with the RNA fold; (iii) presence of two different types of chelated Mg2+ ions; one type helps connect two sequentially nonlocal phosphate groups together (e.g., site 1 Mg²⁺), and the other type connects two sequentially local phosphate groups (e.g., site2 Mg²⁺). The SAM-I aptamer structure, on the other hand, has two partially overlapped domains: the aptamer domain and the expression platform. In general, the aptamer domain has a high binding affinity to small metabolites and accordingly expression platform responds with a large conformational change close to the promotor region of RNA, and this results in gene transcription to be off or on. The ligand/metabolite of this riboswitch is SAM, which is a small co-factor involved in methyl group transfers. In the absence of SAM, a large termination helix formed to activate gene transcription. In the presence of SAM, the aptamer domain forms a very compact conformation that it terminates the transcriptional processes. So far, X-ray crystallography has resolved the structures for the ligandbound aptamer domain of the SAM-I riboswitch from Bacillus subtilis yitJ and Thermoanaerobacter tengcongensis. 48,49 In this study, we have chosen the SAM-I riboswitch aptamer from Thermoanaerobacter tengcongensis as a candidate RNA system.

RNA Preparation. The SAM-I aptamer sequence is derived from the Thermoanaerobacter tengcongensis Met F-Met H2 element. The aptamer sequence used includes sequence additions to the 5' and 3' (before and after P1 helix) to improve primer extension reads. Templates for RNA transcription were prepared as previously described.^{6,7} Polymerase chain reaction was used to prepare transcription templates using Ex-Taq polymerase (TaKaRa) for the amplification of long synthetic templates. Following purification, the transcription templates were transcribed using Ampliscribe highyield transcriptions kits (Epicentre). The RNA was precipitated by the addition of 1 volume of 7 M ammonium acetate and centrifuged. Homogeneity was checked by PAGE (10% polyacrylamide, 7 M urea, 0.5× TBE). Phosphorothioateincorporated aptamers were prepared using the high yield transcription kit. The standard reaction was supplemented by the addition of α -phosphorothioate-NTP (Glen Research) at a 1:20 ratio to its parent NTP (0.375 mM:7.5 mM). After purification, the level of incorporation was verified by 30fluorescent labeling, iodine cleavage, and capillary electro-

Phosphorothioate Interference Mapping. Our expression platform switching assay was used as a selection screen in a phosphorothioate interference assay similar to our previous studies.⁶ Here, aptamer stability is challenged by adding an expression platform oligomer. The oligomer is a chimera of DNA and 2'-O-methyl RNA with the following sequence: [5'-mGmAmA mUmCmU mCdTdC dAdTdC mUmUmU mCmAdG dCdGdA dA-3']. Formation of the expression platform antiterminator helix between the oligomer and the aptamer domain creates a hybrid DNA/RNA duplex. The duplex is a substrate for cleavage by RNase H. Reactions were incubated at 37 °C for 2 h and then purified by high-

performance liquid chromatography (HPLC) (Dionex DNApac column) with 0-40% buffer B (buffer A, 25 mM Tris-HCl pH 8.0, buffer B, 25 mM Tris-HCl pH 8.0 and 1 M NaClO4) in 45 min. The aptamer RNA was randomly incorporated with one of the four α -phosphorothioate-rNTPs. After purification, the RNA was precipitated, and 3'-end was labeled using amine reactive Alexa-488 SPD (Molecular Probes, ~1 mM) in 100 mM NaBO₄ at pH 8.3. Reactions were incubated at room temperature for 6 h, precipitated (3 volumes of ethanol, 300 mM NaOAc at pH 6.5), and purified using the above HPLC gradient to separate labeled from unlabeled. The labeled RNA was then spiked into unlabeled phosphorothioate-incorporated RNA at a level sufficient for capillary electrophoresis analysis following selection. RNA (0.5 mM final concentration) was folded in HMK buffer (containing either 2 mM MgCl₂ or 1 mM MgCl₂ with 1 mM MnSO₄) supplemented with 10, 30, or 100 mM SAM as indicated. After equilibration with RNase H and the chimeric oligomer for 1 h at 37 ° C, the labeled RNA was desalted (micro-biospin P6 columns), lyophilized, and resuspended in Hi-Di formamide. RNase H cleavage removes the label from aptamers unfit to compete for the shared sequence. Populations of each phosphorothioate position are resolved by phosphorothioate cleavage with iodine after selection and analyzed with capillary electrophoresis. Phosphorothioatecontaining diester linkages were cleaved by the addition of 1/10th volume of 100 mM iodine in ethanol and heating to 95 °C for 2 min.

Atomistic Explicit Solvent Simulation Details under Variable RNA Ion-Atmospheric Conditions. Our simulations started with the crystal structure of the SAM-I aptamer (PDB-ID: 2GIS⁹) where two potential chelated Mg²⁺ ions, namely, site1 and site2, already exist. MD simulations of the SAM-I riboswitch were performed first generating the following ion-environment conditions in the presence of metabolite, SAM, at two different temperatures, T = 300 Kand $T^* = 450$ K. The ion-environmental conditions are as follows: (i) (+) Chelated Mg²⁺, (+) 2 mM [Mg²⁺], (ii) (+) Chelated Mg²⁺, (-) 2 mM [Mg²⁺], and (iii) (-) Chelated Mg^{2+} , (-) 2 mM [Mg^{2+}]. However, just to mechanistically understand individual site1 and site2 chelation mediated effects on RNA structure, we have generated two other unphysical situations making one of them absent, each at a time: (iv) (+) site1 Mg²⁺, (-) site2 Mg²⁺ at T^* , (-) 2 mM $[Mg^{2+}]$ at T^* ; (v) (-) site1 Mg^{2+} , (+) site2 Mg^{2+} , (-) 2 mM $[Mg^{2+}]$ at T^* . The control sets of simulations (condition (i)) were prepared under a physiological mixed salt environment where ~ 100 mM [K⁺] and ~ 2.0 mM [Mg²⁺] bulk concentrations were maintained. Physiological bulk concentration generation is a daunting task due to preferential interactions for Mg²⁺ with RNA where in most cases monovalent K⁺ is replaced by Mg²⁺ with its long life-time.³⁰ Due to this preferential interaction, RNA stability is often attributed to the number of excess ions that do not count toward the bulk concentration. This collective excess ion effect is quantified by the preferential interaction coefficient as presented in Tables 1 and 2. Therefore, taking into account all the ion-exchange phenomena and the slow diffusiveness of hexa-hydrated Mg2+, the equilibration method of an RNA system is tricky and needs comprehensive measures where we followed our early established protocol. 30,44

Equilibration Method of the RNA Ion Atmosphere. The equilibration of ion-induced sampling is tricky to obtain

Table 1. Number of Ions Needs to Satisfy the Different Ion-Environment Conditions c

chelated Mg ²⁺	+	+	+	+	-	-
$\begin{bmatrix} Mg^{2+} \end{bmatrix} = 2.0 \\ mM$	+	+	_	_	_	_
$temp \rightarrow$	T	T^*	T	T^*	T	T^*
N_{Mg}^{2+}	11	11	2	2	0	0
N_K^+	116	116	138	138	138	138
N_{Cl}^{-}	46	46	50	50	46	46
$[Mg^{2+}]* mM^a$	2.8	2.86				
[K ⁺]* mM	112	110.3	120.6	117	115.0	116.0
[Cl ⁻]* mM	95	94.9	103.1	103	95.1	99
$[\mathrm{Mg}^{2+}] \mathrm{mM}^{b}$	2.2	2.3				
$[K^{+}]$ mM	100.5	99.5	111.1	109.5	104	107.2
$[Cl^{-}]$ mM	105	104.1	111.1	109.5	104	107.2
$\Gamma_{ m Mg}^{2+}$	9.74	9.69				
$\Gamma_{K}^{^{+}}$	58.59	59.16	74.53	75.58	78.54	76.88
$\Gamma_{ ext{Cl}}^{-}$	-13.98	-13.47	-13.50	-12.42	-13.41	-15.12

"Raw concentration: Raw concentrations are determined 20 Å beyond RNA (asterisk), bCorrected bulk concentrations are determined using a small potential perturbation approximation method. In each condition-dependent simulation, raw salt concentration []* corrected bulk concentrations [] determined (using the aforesaid approach) and calculated preferential interaction coefficients, Γ

Table 2. Number of K^+/Cl^- Ions Needed when Only One/None Site-Specific Chelated Mg^{2+} Present

site1 Mg ²⁺	+	-	
site2 Mg ²⁺		+	
$[Mg^{2+}] = 2.0 \text{ mM}$	-	_	
$temp{\rightarrow}$	T^*	T^*	
$N_{\mathrm{Mg}}^{}^{2+}}$	1	1	
N_K^+	138	138	
$ m N_{Cl}^-$	48	48	
$[Mg^{2+}]* mM^a$			
[K ⁺]* mM	114	115	
[Cl ⁻]* mM	99.2	99.6	
$[\mathrm{Mg^{2+}}] \mathrm{mM}^b$			
$[K^+]$ mM	106.0	106.7	
[Cl ⁻] mM	106.0	106.7	
$\Gamma_{ m Mg}^{2+}$			
$\Gamma_{ m K}^{}$	77.57	76.17	
$\Gamma_{ m Cl}^{-}$	-12.43	-12.83	

"Raw concentration: Raw concentrations are determined 20 Å beyond RNA (asterisk), b*Corrected bulk concentrations are determined using a small potential perturbation approximation method. These are notional ion-environment conditions at high temperature, T^* , purposefully built to understand site-specific chelation effects. In each condition-dependent simulation, raw salt concentration []* corrected bulk concentrations [] determined (using the aforesaid approach) and calculated preferential interaction coefficients, Γ .

the correct distribution of outer-sphere and inner-sphere ions as there is a combination of ions $(K^+; Mg^{2+})$. Here, the challenges are twofold: (i) due to the strong coulombic attraction between the RNA backbone and Mg^{2+} , all Mg^{2+} ions tend to drive fast to condense onto the RNA without forming an appropriate hydration shell; (ii) even if they interact with water, in certain cases, once they stick to a negatively charged RNA site, the potential barrier will not allow it to unbind

easily. In such explicit solvent simulations of RNA, at first, RNA was placed in a waterless box and a required number of ions were added. The ions in our simulations are a combination of excess ions that balance the RNA charge and bulk ions accounting for the physiological ion concentration range. To prevent them from condensing onto the RNA without an appropriate hydration shell, initially, ions were placed randomly with larger van der Waals radii. These ions were equilibrated using stochastic dynamics and a dielectric constant of 80 to mimic water for 10 ns until the electrostatic energy converged keeping RNA frozen. Then, the simulation box was filled with water and annealed to 300 K over 500 ps where RNA and ions were frozen. Following our early protocol, we have first released the Mg²⁺ and equilibrate it for 2 ns and then released RNA where we gradually lowered the position restraining force by 1000, 100, and 0 kcal/mol/ nm² at a constant volume spending 2 ns for each.³⁰ This process collects 10 ns NVT equilibration. Another 10 ns of unrestrained equilibration was added under a constant pressure. As the simulations were conducted under different ionic conditions and temperatures, to maintain the correct density range, the production run was performed under a constant volume. Each of the ionic Individual simulations was 400 ns (3sets each), for a total of 7.2 μ s of sampling that has been performed. In all simulation sets apart from the case of no magnesium ion present, the ligand, SAM, was stably interacting with the RNA (inside the binding pocket near P1-P3 juxtaposition). In general, the time scale of the unbinding/ dissociation rate of SAM is quite large compared to our simulation time scale (in the order of a few ns). This conclusively demonstrates that unrestrained SAM was interacting with the RNA during all the MD production run in all different ion-environmental conditions, except where there was no Mg^{2+} present at the system (in the absence of Site1, Site2 Chelated Mg2+ ions, and 2 mM Mg2+ concentration, only K+ ions are there to stabilize the RNA structure). In this condition, we observed that SAM was disoriented and loosely bound near its binding site.

Parameters. All simulations were performed using the Gromacs version 2018.3. AMBER99 force field⁵⁰ with extensions parmbsc051 and chiOL3.52 The ligand, SAM, is parametrized for AMBER using GAMESS quantum mechanics software 53 and the R.E.D. software package. 54 Atmic charges were calculated using the Restrained ElectroStatic Potential method. 55 The other forcefield parameters were taken from the Generalized Amber ForceField.⁵⁶ The biomolecular force fields, such as AMBER and CHARMM parameters for magnesium, which were used in simulating the riboswitches, result in an exchange rate of water from the first solvation shell that is orders of magnitude smaller than the experimental estimate; the newly derived Mg²⁺ by Villa and co-workers has been used in combination with the TIP3P water model following ref 25. Furthermore, to avoid crystallization at a higher concentration limit, modified K+ parameters were used.⁵⁷ Other than the new Mg²⁺/TIP3P addition, the RNA solution with the updated force field is well tested. 41 While the majority of RNA simulations avoid accounting for direct RNA-ion interactions, our MD simulation protocol predicts stable RNA-Mg²⁺ interaction sites independently, which is validated by our phosphorothioate interference mapping

Quantification of the Preferential Interaction Coefficient of the Ion Atmosphere. The stability of a compact

RNA structure depends on the stability of solution containing associated counter ions. While anions are dispersed in the solution, cations become excess near the RNA over their bulk concentrations. The effect is quantified for ions of species i by the preferential interaction coefficient, Γ_{ij} which depends both on the identity of the RNA and on the bulk concentrations of the ions. The ion-preferential interaction coefficient, $\Gamma_{2+,}$ is defined as $(\partial m_{2+}/\partial m_{RNA})_{\mu 2+}$. m_{RNA} and m_{2+} are the molal concentrations of RNA and divalent ions, I^{2+} , respectively. μ_{2+} is the chemical potential of the divalent metal cation I²⁺. Molal and molar concentrations are effectively the same if the concentration of salt ions and RNA are in the dilute range. The energetic stabilization by I²⁺ is quantified by the I²⁺-RNA interaction free energy. Experimental estimation for Γ^{2+} has been obtained for several systems using the fluorescent dye 8hydroxyquinoline-5-sulfonic acid and other spectroscopic studies. 4,18,58 Γ^{2+} can also be predicted from well-equilibrated explicit-solvent molecular dynamics simulations. $^{30,41}\Gamma$ for any ionic species, i, will be measured as follows: First, the concentration of ionic species will be measured using the time average of the ratio of these molecule counts multiplied by the molarity of pure water.

$$[C_i]^* = 55.51M \frac{N_i}{N_{H_2O}} \tag{1}$$

However, unlike the case near the RNA where ions interact differently with the RNA due to large electrostatic potentials, at 20 Å, the electrostatic potential is under a smooth, small perturbation. Ion densities in a small potential well will respond linearly with their concentration, charge, and the well depth. The corrected bulk concentrations $[C_i]$ (which must be electroneutral) are given by

$$[C_i] = [C_i]^* - q_i [C_i]^* \frac{\sum_j q_j [j]^*}{\sum_j q_j^2 [j]^*}$$
(2)

Here, q_i is the charge, $[C_i]^*$ denotes the raw concentration, and $[C_i]$ denotes the corrected concentration. From the corrected concentration, the preferential interaction coefficients are calculated using the following expression:

$$\Gamma_i = N_i - N_{\rm H_2O} \frac{[C_i]}{55.51M} \tag{3}$$

We found the measurement as shown in Tables 1 and 2 in the Results Section simulating the SAM-I riboswitch aptamer.

In an early study, by performing 2 μ s atomistic explicit solvent molecular dynamics simulations of the SAM-I riboswitch with varying ion concentrations, we have investigated the dynamic interplay between RNA and Mg²⁺ by essentially focusing on the outer-sphere Mg²⁺ ion. As we have increased ion concentrations, we have observed the highly negatively charged RNA to accommodate excess cations its ion-solvation layer over their bulk concentrations.³⁰ We have seen this concentration-dependent ion-solvation redistribution effect also in the SAM-II riboswitch, which accommodates increasing numbers of Mg²⁺ up to a certain Mg²⁺ content.⁴³ Subsequent additions of Mg²⁺ do not effectively add to the 1st layer of Mg²⁺ solvation promoting a saturation effect. While anions are dispersed in the solution, these excess cations substantially contribute toward RNA stabilization and can be measured by experiments.

RESULTS AND DISCUSSION

Phosphorothioate Interference Mapping Experiments and Extensive Atomistic Simulations Identify Inner-Sphere Mg²⁺ Hotspots. The location of each innersphere Mg²⁺ ion is vital for a compact RNA fold. Our phosphorothioate interference mapping experiments help in identifying crucial inner-sphere Mg²⁺ sites prescribing an appropriate distribution of inner- and outer-sphere magnesium ions to maintain a physiological ion concentration of monovalent and divalent salt for the RNA simulation. We have performed phosphorothioate interference mapping experiments in combination with the expression platform switching assay by perturbing the site-specifically bound Mg²⁺ ions (Figure 2). The conformational switching selection

Experiment

PSO₃ interference assay+EP switching assay

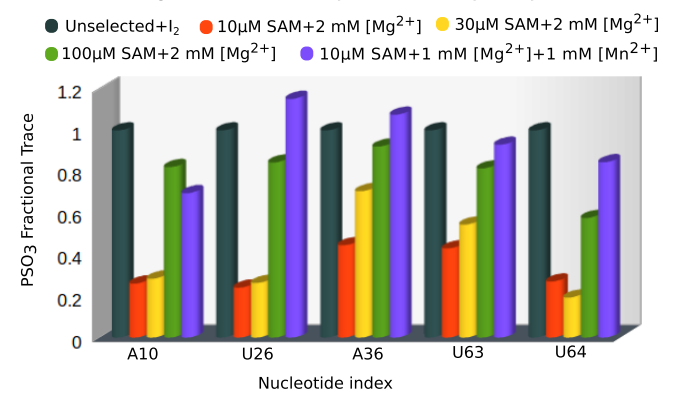


Figure 2. Phosphorothioate interference mapping assay and extended equilibrium simulations together identify potential inner-sphere Mg²⁺ sites.

scheme for phosphorothioate interference is described in the Methods Section. In our experiment, phosphate to phosphorothioate substitution substantially reduces the binding affinity of localized Mg²⁺, which was otherwise closely interacting with the phosphate oxygens of the RNA backbone. In these experiments, aptamer RNA was randomly incorporated with a phosphorothioate nucleotide where we used a level of ~5% with different α -phosphorothioate-NTPs during transcription. The 3' terminus of the RNA was fluorescently labeled and purified. The RNA aptamer was then folded with 2 mM Mg²⁺ and different concentrations of SAM varying from 10 to 100 μM. Selections were performed using RNase H to cleave destabilized aptamers following our previous experimental protocol.⁶ Similar to our earlier work, we have verified the loss of a specific Mg²⁺ interaction by performing a rescue experiment using a buffer with $[Mg^{2+}] = 1$ mM, $[Mn^{2+}] = 1$ mM, and the lowest concentration of SAM (10 μ M). Manganese, being a softer Lewis acid than magnesium, can make more close and stable interaction with the sulfur of the phosphorothioate backbone. By performing capillary electrophoresis following cleavage of the phosphorothioate linkages with molecular iodine, fractional traces of each phosphorothioate position were resolved.

Earlier our experiment found strong interference at A10 and U64 that are anyway connected via site1 chelated Mg²⁺. In addition to those nucleotides, our current assays could capture significant interference at U26 (which belongs to the PK

motif), A36 (which belongs to the kink-turn region), and U63 due to its proximity to U64, which are just beneath the PK motif.

We have performed three independent sets of 1 μ s simulations starting from the crystal structure (pdb:2gis⁹) where two chelated Mg²⁺ (site 1 and site 2) ions pre-exist. In this study, our major concern was to simulate an RNA but under an appropriate ion-environment condition. Each simulation reaches an equilibrium structure where we find three additional inner-sphere Mg²⁺ ions consistently reach near U26, A36 location as we find in the experiment (Figure S1). Although our phosphorothioate interference mapping experiments were adept in identifying most of the inner-sphere Mg²⁺, we did not find significant interference at A84 and A85 locations where the crystal structure found a potential chelated Mg²⁺ binding site as interference will only arise if only the pro-Rp oxygen interacts with the Mg.⁶ This certainly raises a question regarding the binding affinity and the impact of site2chelation center on RNA structure stabilization.

Phosphorothioate interference mapping experiments show positions where interference is high. Capillary electrophoresis traces of selected and unselected RNA are included with ATP α S. To fold the RNA, various concentrations of SAM were taken and a rescue operation is also performed with 1 mM Mn²⁺ along with 1 mM Mg²⁺ keeping minimum SAM concentration (10 μ M). Electropherograms for the UTP α S interference assay are shown elsewhere. Traces are integrated, and the areas are normalized to peaks that display no selection. As the concentration of SAM increases, the trace population of phosphorothioate returns to normal.

Preferential Interaction Coefficients Quantitatively Characterize the RNA Ion Environment. The physiological ion environment of RNA is an extremely complex environment due to the presence of multiple essential entities involving Mg²⁺, K⁺, Cl⁻, and water. In addition, various complex physical phenomena, like counter-ion condensation, chelation, and ionpair effect including other electrostatic coupling effects, make it extremely challenging to isolate the contribution from any one or two species toward RNA structural stabilization. While our phosphorothioate interference mapping assay suggests that the chelated Mg²⁺ at site1 may impart a significant stabilization effect to the RNA core, it does not pinpoint which RNA interactions are most sensitive to the chelation effect.

As mentioned before, due to the slow timescale issue, it is a daunting task to capture RNA conformational degrees of freedom by any canonical simulations at room temperature. Consequently, any free energy simulations along the one/two order parameter plane are also challenging knowing the fact that RNA conformational change is a multidimensional problem. Hence, we decided to minimally perturb the system by imposing the high-temperature effect making the system moderately flexible such that we can isolate RNA's structural sensitivity toward different ion environments. To precisely capture the effect of inner- and outer-sphere ionic effects on RNA conformations, we have first generated three independent ion-environmental conditions individually at two different temperatures, referring to T = 300 K and $T^* = 450 \text{ K}$. The ionenvironmental conditions are as follows: (i) (+) Chelated Mg^{2+} , (+) 2 mM [Mg^{2+}]; this is a reference system where the SAM-I aptamer includes the presence of site1, site2 chelation maintaining a 2 mM Mg^{2+} concentration. (ii) (+) Chelated Mg^{2+} , (-) 2 mM $[Mg^{2+}]$; this is to understand the impact of two chelated Mg2+ ions and their coupled behavior in the

absence of any outer-sphere/bulk Mg^{2+} . Here, K^+ only helps in maintaining a neutralized ion-environment condition. (iii) (–) Chelated Mg^{2+} , (–) 2 mM $[Mg^{2+}]$; this is an extreme condition, which is generated where there is no Mg^{2+} at all; only K^+ ions are there to stabilize the RNA structure.

In an early study, we have observed the highly negatively charged RNA to accommodate excess cations in its ionsolvation layer over their bulk concentrations. This excess cationic effect can efficiently be characterized both theoretically and experimentally by quantifying the preferential interaction coefficient, (Γ_i) . The definition and calculation methods are described in the Methods section where we have depicted how we have obtained a corrected electroneutral bulk concentration as enlisted in Table 1. We observe a $\Gamma_{\rm Mg}^{2+}$ of 9.74 at 2 mM [Mg²⁺] with the new Mg²⁺ parameters in the context of a nucleic acid reported by Villa and co-workers, while earlier our predictions were based on Mg²⁺ parameters by Åqvist where the Mg²⁺-water exchange rate was underestimated by several orders of magnitude. ^{25,59} In Mg²⁺-RNA titration experiments, for adenine-binding and other riboswitch systems, it is shown that $\Gamma_{\rm Mg}^{\ \ 2+}$ significantly varies its magnitude depending on its conformational state. 4,11 Although we have chosen particularly a high temperature (450 K) to accelerate the slow conformational change by enhancing the rate of Mg²⁺-water exchange, the enhanced rate, however, marginally affects $\Gamma_{\rm Mg}^{2+}$. At the higher temperature of 450 K, we find $\Gamma_{\rm Mg}^{2+}$ of 9.69, which does not deviate much from the value we find at 300 K. This signifies that in the presence of both chelated, inner- and outer-sphere Mg²⁺ ions, except local, large conformational changes are less probable at 450 K within our simulation timescale. Thus, we can consider the ion environment of RNA at $T^* = 450 \text{ K}$ as a new reference set with which other ionic conditions at the same temperature can be compared. In other ionic conditions, where only chelated Mg²⁺ ions are present, the calculation of $\Gamma_{\rm Mg}^{\ \ 2+}$ is irrelevant and left out. However, just to mechanistically understand individual site1 and site-2 chelation mediated effects on RNA structure, we have generated two other unphysical situations making one of them absent, as a separate event. In this situation, a substantial number of K+ ions are accommodated in the ionsolvation layer of RNA reflected in the calculation of Γ_{K}^{+} , while Cl⁻ ions stay dispersed, shown in Table 2.

Contact Probability Maps Isolate the Macroscopic Structural Impact of Mg²⁺ Chelation. The preferential interaction coefficient and its change are mostly affected by the outer-sphere Mg²⁺ than site-specifically bound Mg²⁺, which are strongly bound to the phosphate groups of RNA. However, these site-specifically bound inner-sphere/chelated ions have the tremendous potential not only to reorganize its local ion density of outer-sphere Mg2+ /K+, but their presence or absence can also control the global conformational dynamics of RNA. Here, we monitor and compare the RNA conformational dynamics by generating contact probability maps (CPMs) for the different ion-environmental conditions as shown in Figure 3. From our CPM analysis comparing the conformational changes at two different temperatures (T and T*), each under the ionic environment of 2 mM [Mg²⁺] and 100 mM [K⁺], we find the RNA only to instigate a slight local conformational fluctuation at the referred higher temperature (Figure 3a,b). At this temperature limit when we analyze an unphysical condition keeping only two chelated Mg2+ at 100 mM [K+], we observe a noticeable change in the P1 and P3 juxtaposition. Early small angle X-ray scattering and fluorescence resonance

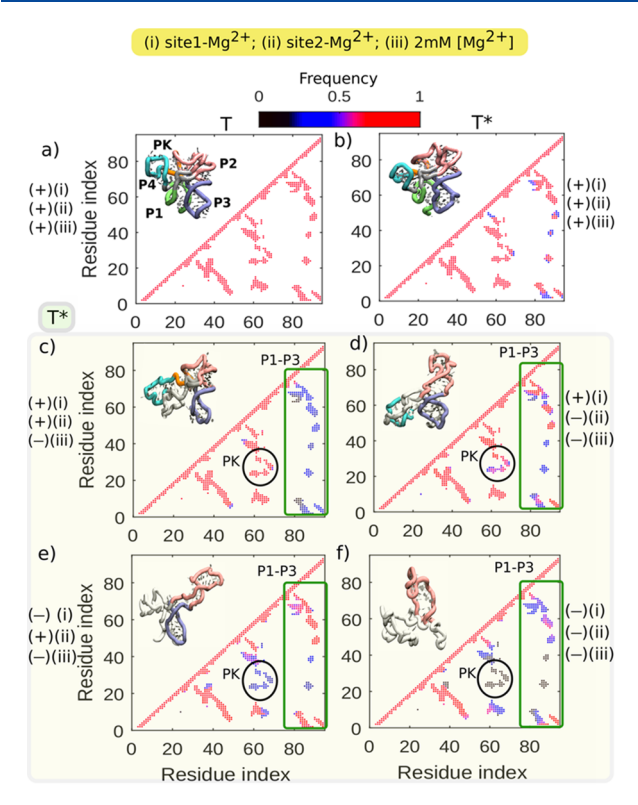


Figure 3. Contact probability maps detect RNA pseudoknot (PK) deformation in the absence of Mg²⁺ chelation. Contact probability maps are analyzed comparing the following ionic conditions: (a) In the presence of site1 and site 2 chelated magnesium ions and outersphere ions maintaining 2 mM [Mg²⁺] (this is a controlled condition at 300 K). (b) Same as (a) but at a stimulating temperature (T^* = 450 K); (c) in the presence of site1 and site2 but in the absence of outer-sphere Mg²⁺ ions maintaining a 2 mM [Mg²⁺]; (d) in the absence of outer-sphere and site2 chelated Mg²⁺ ions but the presence of site1 chelated Mg2+ ions. (e) In the absence of outer-sphere and site1 chelated Mg²⁺ ions but the presence of site2 chelated Mg²⁺ ions, only. (f) No Mg²⁺ present. Residue-level contact probability for each of these variable conditions (bottom) is compared with that of the controlled condition where $\sim 2.0 \text{ mM} \left[\text{Mg}^{2+}\right]$ and $100 \text{ mM} \left[\text{K}^{+}\right]$ are maintained at 300 K. A remarkable difference is detected near the PK region (residue index (RI): 65-68; 25-28) if any/both the chelated Mg²⁺ ions are removed.

energy transfer (FRET) experiments including our early structure-based electrostatic simulations of the SAM-I aptamer show the involvement of both metabolite and magnesium ions in the structural stabilization of the P1-P3 juxtaposition. 8,47,60 This juxtaposition secures SAM-binding elements, P1 and P3. Our early atomistic molecular simulations study explained the integrated role of metabolite (SAM) and Mg²⁺ mechanistically where we found that SAM essentially connects the P1-helix with P3, where the independent effect of small, dynamic Mg²⁺ is not sufficient to make this connection stable due to the high degree of flexibility of the 5'-end of P1-helix. The same argument holds for metabolite alone where the independent effect of SAM is not sufficient to connect P1 and P3 connection as it costs a huge electrostatic barrier. In the present study, while metabolite is present in its binding pocket, due to the absence of 2 mM [Mg²⁺] (major constituents are a collection outer-sphere Mg²⁺ ions), we have observed the significant deformation in the P1-P3 tertiary interaction disrupting the binding pocket (Figure 3c). This is consistent with our early simulation study, which accounts only for outersphere Mg^{2+} ions.⁴⁷ Subsequently, when we removed the exposed chelated- Mg^{2+} from the site2, we observed some of the pseudoknot contacts connecting P2 and P4 helices become highly sensitive (Figure 3d,e). This sensitivity becomes severe when the core-chelated- Mg^{2+} is removed from site 1. As a result, most of the pseudoknot contacts are deformed and an extended RNA conformation is formed. Under another extreme condition when this RNA system is projected to a no Mg^{2+} condition, a residual portion of secondary structure from P2 and P4 is the only survivor motifs in the structure (Figure 3f). However, our CPM analysis performed at room temperature ($T=300~\mathrm{K}$) detects no significant structural changes. This is a consequence of the slow kinetics of RNA fluctuations (Figure S2).

Mg²⁺ Chelation Modulates RNA Fluctuation by Terminating Tertiary Pseudoknot Connection. Earlier, by single-molecule FRET (smFRET) and our various structure probing experiments including nucleotide analog interference mapping (NAIM), 2-aminopurine switching assay, ligand titration, and SHAPE probing, we have observed that Mg²⁺ binding to the aptamer promotes the formation of the pseudoknot interaction. 5-8 However, from all these experiments, it is difficult to pinpoint whether the stabilization results from any site-specifically bound Mg²⁺ or from the collective effect of outer-sphere Mg²⁺. In our simulations, as the Mg²⁺ ion-environment changes, a measurable effect on RNA fluctuations is expected. To characterize this dynamical effect of the RNA, we have calculated the average root mean square fluctuation (RMSF) along with a residue index under varying ionic conditions (Figure 4a). It is expected that P1 being a terminal helix shows large RMSF values. However, it is a highly nontrivial outcome that as we impose a condition like one or no Mg²⁺, which means when we remove any of chelated Mg²⁺ or both at a time, the PK tertiary interaction consistently shows high RMSF compared to other nonterminal location of the RNA. This indicates that the presence of both the chelated is required in securing the pseudoknot connection (Figure 4b,c). This coupled effect is very analogous to the AND gate of the digital logic gate concept that helps to understand the binary input-output mechanism of electronic devices. The AND gate results in a HIGH output only if all the inputs to the AND gate are HIGH. Now when one looks back to Figure 1c, it becomes clearer that if we imagine the SAM-I aptamer as an RNA device, the presence of both the chelated Mg²⁺ ions is required as a support-gate of the pseudoknot fold (Figure 4d).

Chelation Induces Dynamical Anticorrelation between PK and P1-P3 Tertiary Junctions. The importance of PK specifically on SAM-I structure-function has been elucidated in several experimental studies, whereas the tertiary PK motif is distantly located from the metabolite binding site. 5-9,61 Despite its distant location, the formation of the PK was found crucial for ligand binding and riboswitch activity. The functional impact of PK was more established where using in vitro transcription assays the wild-type riboswitch is compared with the G55C/G56C mutant. It was found that the riboswitch activity is severely affected by the disruption of the pseudoknot even in the presence of SAM.8 Also, these studies found that disruption of the pseudoknot interaction instigates the deformation of the P1-P3 close juxtaposition. Consistent with these early smFRET results, we have also observed an intricate interplay between these two tertiary motifs (PK connection and P1-P3 connection) (Figure 5). PK is essentially a long-range tertiary connection between the PK

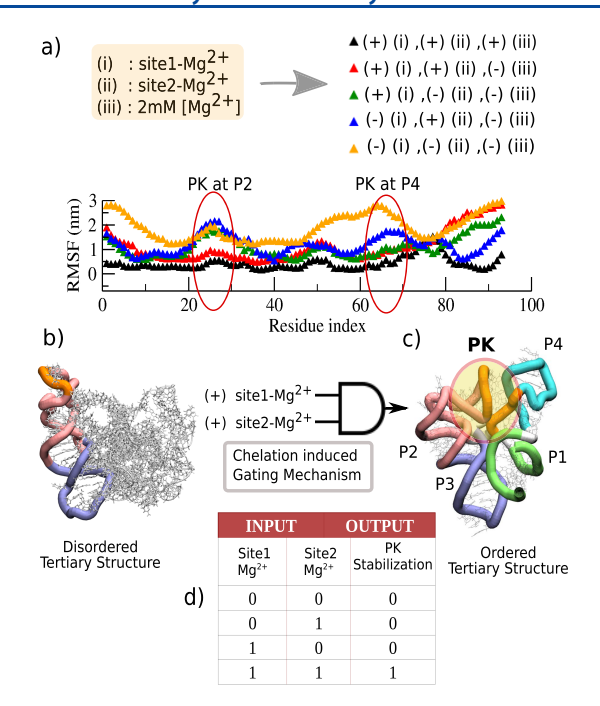


Figure 4. (a) Root mean square fluctuation (RMSF) measurements capture the amplified flexibility of the PK region. RMSF calculations have been performed accounting backbone phosphate groups under four most sensitive conditions: (color code: red, green, blue, and yellow) in comparison to the controlled condition (black). RMSF change reflected the near PK region (r25-r28) close to the P2 helix when any/both chelated magnesium is removed. RMSF amplified the near PK region (r65-r68) close to P4 specifically when core chelated Mg²⁺ is removed. (b) RMSF calculation identified two prime sensitive nonlocal tertiary interactions: PK and P1-P3 junction, which are deformed when any/both chelated Mg2+ disappear. (c) Stabilization of PK and P1-P3 juxtaposition explicitly requires support from both the chelated Mg²+ ions, in a site-specific way. (d) This collective input effect of two chelated Mg²+ ions in the stabilizing of the PK device of RNA represents a biological analog of binary 'AND' logic Gate, which promotes the high output as a result of all high from all inputs.

segment near P2 (indicated as PK P2) and the PK segment near P4 (indicated as PK P4). At the physiological ionic environment ($[Mg^{2+}] \sim 2.0$ mM, $[K^+] \sim 100$ mM), we have observed a weak anticorrelated pattern in the dynamics of PK and P1-P3 connecting distances (Figure 5a) (correlation coefficient ~ -0.3). This steady anticorrelated dynamical flow is disturbed when we eliminate any important ion component/ s from its ion atmosphere. If we eliminate all the outer-sphere Mg²⁺, the time-dependent distance profile clearly shows the most affected P1-P3 juxtaposition (Figure 5b). Again, when we eliminate any of the chelated Mg²⁺ (site1/site2) or both the chelated Mg²⁺ ions, we immediately observe the deformation of PK (Figure 5c,d). Almost in every case, when we remove the chelated Mg²⁺, we observe that PK deformation is followed by P1-P3 deformation (Figure 5c-e). This observation correlates well with the same observed in the early smFRET experiment.8

Chelation Safeguards Nonlocal Base-Triple to Inhibit Large-Scale PK Deformation. As illustrated in Figure 1, it appears from the crystal structure of the SAM-I riboswitch that the site1 and site2 chelated Mg²⁺ ions are located in such a way that they can safeguard the base-pair formation between A85 and U64. On the other hand, our ionic condition-dependent analysis shows in the absence of chelated Mg²⁺ a large-scale

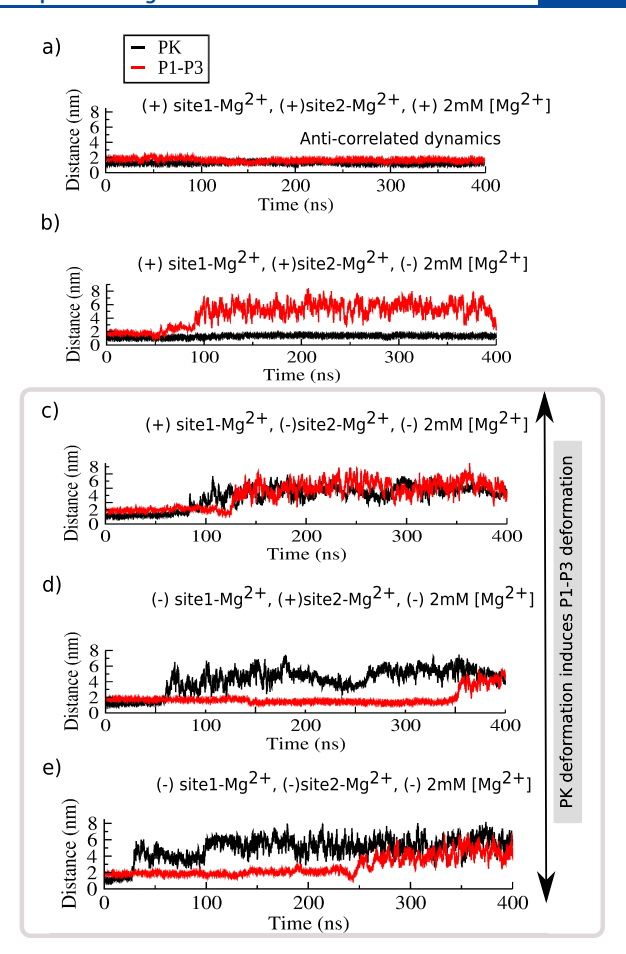


Figure 5. Two important tertiary connections, PK and P1–P3 helical juxtaposition in SAM-I show anticorrelated dynamical behavior. Distance trajectories for nonlocal PK connection and P1–P3 connection under different ion-atmospheric conditions as labeled: (a) (+) site1 $\mathrm{Mg^{2^+}}$, (+) site2 $\mathrm{Mg^{2^+}}$, (+) 2 mM [$\mathrm{Mg^{2^+}}$]; (b) (+) site1 $\mathrm{Mg^{2^+}}$, (-) 2 mM [$\mathrm{Mg^{2^+}}$]; (c) (+) site1 $\mathrm{Mg^{2^+}}$, (-) site2 $\mathrm{Mg^{2^+}}$, (-) 2 mM [$\mathrm{Mg^{2^+}}$]; (d) (–) site1 $\mathrm{Mg^{2^+}}$, (+) site2 $\mathrm{Mg^{2^+}}$, (-) 2 mM [$\mathrm{Mg^{2^+}}$]. Here, all the dynamics were analyzed under T^* (450 K) temperature. P1–P3 connection is found to be sensitive toward outersphere $\mathrm{Mg^{2^+}}$ ions. PK connection shows its sensitivity toward chelation effects. In most of the ionic conditions, P1–P3 shows a higher flexibility, and metabolite exploits this connection in order to switch transcription ON/OFF. Chelation guards the residual RNA fold both in ON and OFF states.

deformation in the PK region. Although U64 is an adjacent base of the PK region, the question yet to be answered, which microscopic event/mechanism instigates such a large deformation in PK, thereby promoting the global unfolding of the RNA. To understand this, we have performed a normal mode analysis, which helps us to explore the correlated motion between different distant dynamic regions/domains in this RNA. The lowest and most correlated modes are shown with the directions of motion along with the normal mode in Figure 6a (in the presence of all ions including chelation) and Figure 6b (in the absence of site1/core chelated Mg²⁺). We have also analyzed the pairwise cross-correlation maps (Figures S3-S5). Both the analyses capture large-scale PK breathing dynamics, which is governed by the correlated dynamics between distant P2 and P4 helices. After investigating all the modes, we find that the epicenter of the dynamical correlation under the effect

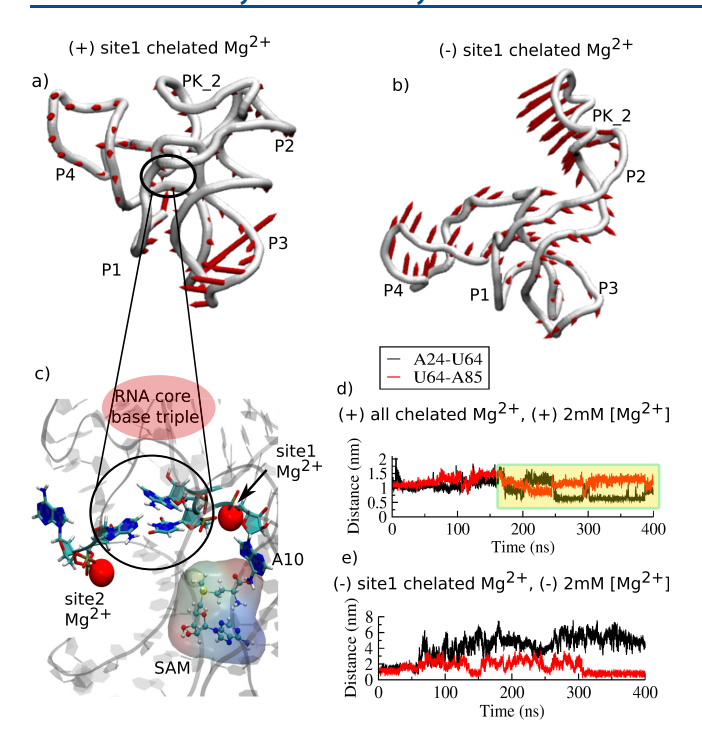


Figure 6. Normal mode analysis pinpoints a competitive nonlocal base-triple and their anticorrelated dynamics safeguard the tertiary fold of PK. From normal mode analysis, only the lowest frequency mode along the direction of motion is shown for (a) in the presence of site1 chelated Mg2+ (all ion components present) and (b) in the absence of site1 chelated Mg²⁺. This lends support to the large-scale PK breathing motion in the absence of site1 Mg²⁺. (c) Competitive base-triple A24-U64-A85 at the RNA core is found to dictate the deformation of PK and P1-P3 long-range tertiary interactions. (d) When all ion components are present (the controlled condition) including core/site1 Mg²⁺, an anticorrelated dynamical behavior is observed in distances between A24-U64 and A85-U64. (e) In the absence of core/site1 Mg²⁺, A24-U64 breaks, immediately resulting in PK opening, which is followed by the separation of A85-U64 leading to P1-P3 deformation. This example explicitly shows how the relevant microscopic fluctuation amplifies and transmits to cause global conformational changes in RNA.

of chelation lies beneath a competitive base-triple where A85, U64 forms a triple-connection with A24 (Figure 6c). This is an event of love-triangle where A24 and A85 compete for U64. This competition is exhibited in their anticorrelated dynamical behavior even when we monitor the distance-time trajectory of A24-U64 and U64-A85 (Figure 6d). When we remove any of site1/site2 chelated Mg²⁺, this microscopic fluctuation around this base-triple amplifies, and A24-U64 (close to PK) breaks and instigates a large change in the PK region (Figure 6e). In most of our trajectories, we have observed the deformation of the P1-P3 connection, affecting SAM binding, when the U64-A85 connection breaks. On the other hand, chelation-induced A24-U64 deformation affects PK folding. As a result of PK deformation, ultimately the RNA core gets exposed (Figure 6b). However, we did not notice any noticeable influence of SAM in our simulation sets under varying ionic conditions where it mostly stays in its active site except in the absence of Mg²⁺. A future atomistic study is necessary to understand the influence of the ligand in connection to the chelation effect.

CONCLUSIONS

A nucleic acid system operates its biological function when it acquires a suitable functional ambiance. That ambiance is created by its ion atmosphere, a multilayered sheath surrounding this highly charged polymer. The ion atmosphere is composed of different types of ions. Some decide to interact with RNA directly (site bound ion, other inner-sphere ions), some interact indirectly screened by water (outer-sphere ions), and some stay diffused (mostly in a hexa-hydrated form).³ The transformation of a particular ion to any of these interactive forms occurs through the hydration/dehydration process to interact with RNA, which then governs the structure, dynamics, and thermodynamics of the RNA-ion complex. The mode of transformation of the ion cloud is again wellcorrelated with the functional fold of RNA to perform specific activities. In the present case, the SAM-I riboswitch functions in the transcription regulation process by transforming between its ON and OFF alternative folds not only in the presence of metabolite, but these folds have their independent Mg²⁺ concentration dependence. This we have explicitly observed in our early experimental and simulation studies by analyzing the population profile of the transcription-OFF/ transcription-ON as a function of [Mg²⁺].⁴² It reveals that the ratio is maximized at an intermediate Mg2+ concentration of 4.0 mM Mg²⁺. Beyond this concentration, the stability of the expression platform starts to enhance at the cost of aptamer stability, specifically by affecting P1 and P4 helices. However, even in this transcription-ON state, a residual RNA tertiary fold stays intact at the aptamer level where the tertiary PK region remains protected to perform the required function in the transcription activation process. Here comes the functional role of chelated Mg²⁺ in stabilizing an active fold of RNA, the current study reveals. Below we summarize the key highlights of this study and new findings on the role of ion chelation effects on RNA structure:

- (i) The present study attempts here to mimic the mixed salt environment with a correct bulk concentration of K⁺, Mg²⁺, and Cl⁻ guided by the calculations of the preferential interaction coefficient, which quantitatively captures the heterogeneity in the RNA ion solvation layer (Table 1). In simulation studies, the assessment of correct bulk concentration is essentially attributed to the correct distribution of inner- and outer-sphere ions. Mg²⁺ being an effective modulator of the RNA ion environment, the number of inner-sphere Mg²⁺ ions and their site dependence are corroborated by our phosphorothioate interference mapping experiments of the SAM-I aptamer.
- (ii) Our phosphorothioate interference mapping and crystallographic data reveal the presence of two primary chelated Mg²⁺ ions: one residing at the core connecting two nonlocal (in sequence) phosphate groups in the backbone (near 4-way helical junction) and the other is rather exposed connecting two local (in sequence) phosphate groups (near 1–4 helical-stack region).
- (iii) To understand the structural and functional importance of these chelated Mg²⁺ ions in stabilizing the RNA core, we have created different ion-atmospheric conditions including a control one as a reference and two unphysical situations at high temperature solely to understand site-specific chelation effects on RNA. All together when we compare and analyze the RNA

structure under such ion-atmospheric conditions, we find the importance of outer-sphere Mg2+ in stabilizing the flexible P1-P3 helical juxtaposition that controls the switching of the transcription activation process by shifting the population from the stable aptamer to the stable expression platform. In the current study, the key finding is the central role of chelated Mg2+ ions in stabilizing the pseudoknot motif of the SAM-I aptamer. Our CPM (Figure 3) indeed shows that while two specific chelated Mg²⁺ ions are responsible for stabilizing the PK motif bringing P2 and P4 helices together, outersphere/diffuse Mg²⁺ ions exert significant stabilization effects over the flexible P1-P3 helical junction (Figure 5b). The importance of Mg²⁺ ions in stabilizing the PK motif has been observed in several early experiments that created a no-Mg²⁺ ionic condition. 5-7 To further address this point, we would like to emphasize that in various experiments, such as single-molecule FRET (smFRET), NAIM, 2-aminopurine switching assay, ligand titration, and SHAPE probing, it is observed that Mg²⁺ ions binding to the aptamer promote the formation of the pseudoknot (PK) interactions.^{5–8} However, from all these experiments, it is difficult to conclude whether the stabilization of the PK interaction comes from the sitespecifically bound Mg²⁺ or from the collective effects of outer-sphere Mg²⁺/diffused Mg²⁺. From our study, we could distinguish that the Site1/Core chelated Mg²⁺, which is essentially coordinating two nonlocal phosphates groups, A10 (belongs to the P2 region) and U64 (in the P4 helix) through strong electrostatic interactions, helps to bring two large distant helices P2 and P4 close to form the PK. In fact, both the site-specific chelated Mg²⁺ ions (Site1 and Site2) mechanistically control structural stabilization of the PK motif, which is evident from our rigorous analysis of CPMs (Figure 3cf), RMSF calculations (Figure 4a), distance trajectories of nonlocal PKs, and P1-P3 connections (Figure 5c-e) under different physiological ionic conditions. Most importantly, we find the microscopic basis of the PK stabilization where two competitive base pairs (A24-U64 and U64-A85) in a base triple A24-U64-A85 play a crucial role in PK stabilization (Figure 6e). This is also verified by our normal mode analysis (Figure 6b). We have also observed that the chelated Mg2+ ioninduced PK stabilization supports the RNA core in such a way that its deformation instigates the deformation of all the tertiary interactions including the P1-P3 helical juxtaposition. In close connection with these observations, the early smFRET result correctly pointed out that PK supports the idea that it may be used as a lever to correctly position P3 close to P1, via the P2-P3 helical stacking. 9,60,62 Although it is a distant tertiary motif, it can severely affect the metabolite binding at the P1-P3 junctional region and in turn the transcription activation process. This is excellent functional evidence of allosteric regulation in RNA via PK.

In connection with all experimental and simulation results, at this far, we understand the functional role of PK where it helps tightly pack the RNA core of the aptamer. The stability of PK gravely depends on the chelated Mg²⁺. Most importantly, we find that the placement of two chelated Mg²⁺ ions is highly crucial; they work in concert to support the

long-range PK connection. We have observed ripped PK if any one of chelated $\mathrm{Mg^{2+}}$ disappears. This outcome is analogously found in the binary AND logic gate where all the high inputs are necessary to get an output. This describes the collective effect of two chelated $\mathrm{Mg^{2+}}$ ions following a gating mechanism that supports the close-packed RNA core of the SAM-I aptamer.

RNA aptamers have already entered the clinical pipeline in virus detection and antiviral therapy, along with more than nine ongoing clinical trials for various types of cancer, coronary artery bypass graft surgery. A detailed thermodynamic understanding of the chelation effect will indeed enable greater control of aptamer/riboswitch regulation. This study anticipates the chelation concept to uphold an upcoming technology in the application of RNA aptamer-based virus detection and therapeutics.

ASSOCIATED CONTENT

Supporting Information

The Supporting Information is available free of charge at https://pubs.acs.org/doi/10.1021/acs.jpcb.1c02467.

Equilibrium structure of SAM-I identifying inner-sphere Mg²⁺ locations; characterization of RNA conformations under different ionic conditions at 300 K; normal mode analyses; and Figures S1–S5 (PDF)

Special Issue Paper

This paper was intended for the Lawrence R. Pratt Festschrift Virtual Special Issue, published May 20, 2021.

AUTHOR INFORMATION

Corresponding Authors

José N Onuchic — Center for Theoretical Biological Physics and Departments of Physics and Astronomy, Chemistry, and Biosciences, Rice University, Houston, Texas 77005, United States; orcid.org/0000-0002-9448-0388; Email: jonuchic@rice.edu

Karissa Y Sanbonmatsu — Theoretical Biology and Biophysics Group, Theoretical Division, Los Alamos National Laboratory, Los Alamos, New Mexico 87545, United States; New Mexico Consortium, Los Alamos, New Mexico 87544, United States; orcid.org/0000-0002-7965-7392; Email: kys@lanl.gov

Susmita Roy — Department of Chemical Sciences, Indian Institute of Science Education and Research Kolkata, Kolkata, West Bengal 741246, India; orcid.org/0000-0001-6411-4347; Email: susmita.roy@iiserkol.ac.in

Authors

Raju Sarkar – Department of Chemical Sciences, Indian Institute of Science Education and Research Kolkata, Kolkata, West Bengal 741246, India

Akhilesh Jaiswar – Department of Chemical Sciences, Indian Institute of Science Education and Research Kolkata, Kolkata, West Bengal 741246, India

Scott P Hennelly — Theoretical Biology and Biophysics Group, Theoretical Division, Los Alamos National Laboratory, Los Alamos, New Mexico 87545, United States; New Mexico Consortium, Los Alamos, New Mexico 87544, United States

Complete contact information is available at: https://pubs.acs.org/10.1021/acs.jpcb.1c02467

Notes

The authors declare no competing financial interest.

ACKNOWLEDGMENTS

R.S., A.J., and S.R. thank DIRAC supercomputing facility at IISER-Kolkata for computational support. S.R. acknowledges support from the Department of Biotechnology (DBT) (Grant No. BT/12/IYBA/2019/12) and Science and Engineering Research Board (SERB), Department of Science and Technology (DST), Govt. of India (Grant No. SRG/2020/001295). J.N.O. and K.Y.S. acknowledge NIH NIGMS grant R01GM110310.

REFERENCES

- (1) Nguyen, H. T.; Thirumalai, D. Charge Density of Cation Determines Inner versus Outer Shell Coordination to Phosphate in RNA. *J. Phys. Chem. B* **2020**, *124*, 4114–4122.
- (2) Kolev, S. K.; Petkov, P. S.; Rangelov, M. A.; Trifonov, D. V.; Milenov, T. I.; Vayssilov, G. N. Interaction of Na(+), K(+), Mg(2+) and Ca(2+) counter cations with RNA. *Metallomics* **2018**, *10*, 659–678
- (3) Draper, D. E. A guide to ions and RNA structure. RNA **2004**, *10*, 335–343
- (4) Grilley, D.; Misra, V.; Caliskan, G.; Draper, D. E. Importance of partially unfolded conformations for Mg(2+)-induced folding of RNA tertiary structure: structural models and free energies of Mg2+ interactions. *Biochemistry* **2007**, *46*, 10266–10278.
- (5) Eschbach, S. H.; St-Pierre, P.; Penedo, J. C.; Lafontaine, D. A. Folding of the SAM-I riboswitch: a tale with a twist. *RNA Biol.* **2012**, 9, 535–541.
- (6) Hennelly, S. P.; Novikova, I. V.; Sanbonmatsu, K. Y. The expression platform and the aptamer: cooperativity between Mg2+ and ligand in the SAM-I riboswitch. *Nucleic Acids Res.* **2013**, *41*, 1922–1935.
- (7) Hennelly, S. P.; Sanbonmatsu, K. Y. Tertiary contacts control switching of the SAM-I riboswitch. *Nucleic Acids Res.* **2011**, *39*, 2416–2431.
- (8) Heppell, B.; Blouin, S.; Dussault, A. M.; Mulhbacher, J.; Ennifar, E.; Penedo, J. C.; Lafontaine, D. A. Molecular insights into the ligand-controlled organization of the SAM-I riboswitch. *Nat. Chem. Biol.* **2011**, *7*, 384–392.
- (9) Montange, R. K.; Batey, R. T. Structure of the S-adenosylmethionine riboswitch regulatory mRNA element. *Nature* **2006**, 441, 1172–1175.
- (10) Romer, R.; Hach, R. tRNA conformation and magnesium binding. A study of a yeast phenylalanine-specific tRNA by a fluorescent indicator and differential melting curves. *Eur. J. Biochem.* 1975, 55, 271–284.
- (11) Leipply, D.; Draper, D. E. Effects of Mg2+ on the free energy landscape for folding a purine riboswitch RNA. *Biochemistry* **2011**, *50*, 2790–2799.
- (12) Koculi, E.; Hyeon, C.; Thirumalai, D.; Woodson, S. A. Charge density of divalent metal cations determines RNA stability. *J. Am. Chem. Soc.* **2007**, *129*, 2676–2682.
- (13) Christian, J. H. B.; Waltho, J. A. The sodium and potassium content of non-halophilic bacteria in relation to salt tolerance. *J. Gen. Microbiol.* **1961**, 25, 97–102.
- (14) Grover, N. On using magnesium and potassium ions in RNA experiments. *Methods Mol. Biol.* **2015**, *1206*, 157–163.
- (15) Nguyen, H. T.; Hori, N.; Thirumalai, D. Theory and simulations for RNA folding in mixtures of monovalent and divalent cations. *Proc. Natl. Acad. Sci. U. S. A.* **2019**, *116*, 21022–21030.
- (16) Callahan, K. M.; Casillas-Ituarte, N. N.; Roeselová, M.; Allen, H. C.; Tobias, D. J. Solvation of magnesium dication: molecular dynamics simulation and vibrational spectroscopic study of magnesium chloride in aqueous solutions. *J. Phys. Chem. A* **2010**, 114, 5141–5148.

- (17) Dudev, T.; Lim, C. Importance of metal hydration on the selectivity of Mg2+ versus Ca2+ in magnesium ion channels. *J. Am. Chem. Soc.* **2013**, 135, 17200–17208.
- (18) Grilley, D.; Soto, A. M.; Draper, D. E. Mg2+-RNA interaction free energies and their relationship to the folding of RNA tertiary structures. *Proc. Natl. Acad. Sci. U. S. A.* **2006**, *103*, 14003–14008.
- (19) Conn, G. L.; Gittis, A. G.; Lattman, E. E.; Misra, V. K.; Draper, D. E. A compact RNA tertiary structure contains a buried backbone-K + complex. *J. Mol. Biol.* **2002**, *318*, 963–973.
- (20) Draper, D. E. RNA folding: thermodynamic and molecular descriptions of the roles of ions. *Biophys. J.* **2008**, *95*, 5489–5495.
- (21) Misra, V. K.; Draper, D. E. A thermodynamic framework for Mg2+ binding to RNA. *Proc. Natl. Acad. Sci. U. S. A.* **2001**, 98, 12456–12461.
- (22) Leipply, D.; Draper, D. E. Evidence for a thermodynamically distinct Mg2+ ion associated with formation of an RNA tertiary structure. J. Am. Chem. Soc. 2011, 133, 13397–13405.
- (23) Tan, D.; Piana, S.; Dirks, R. M.; Shaw, D. E. RNA force field with accuracy comparable to state-of-the-art protein force fields. *Proc. Natl. Acad. Sci. U. S. A.* **2018**, *115*, E1346–E1355.
- (24) Yu, T.; Chen, S. J. Hexahydrated Mg(2+) Binding and Outer-Shell Dehydration on RNA Surface. *Biophys. J.* **2018**, *114*, 1274–1284.
- (25) Allnér, O.; Nilsson, L.; Villa, A. Magnesium Ion-Water Coordination and Exchange in Biomolecular Simulations. *J. Chem. Theory Comput.* **2012**, *8*, 1493–1502.
- (26) Ramesh, A.; Wakeman, C. A.; Winkler, W. C. Insights into metalloregulation by M-box riboswitch RNAs via structural analysis of manganese-bound complexes. *J. Mol. Biol.* **2011**, *407*, 556–570.
- (27) Rangan, P.; Woodson, S. A. Structural requirement for Mg2+binding in the group I intron core. J. Mol. Biol. 2003, 329, 229–238.
- (28) Ren, A.; Rajashankar, K. R.; Patel, D. J. Fluoride ion encapsulation by Mg2+ ions and phosphates in a fluoride riboswitch. *Nature* **2012**, *486*, 85–89.
- (29) Manning, G. S. The molecular theory of polyelectrolyte solutions with applications to the electrostatic properties of polynucleotides. *Q. Rev. Biophys.* **1978**, *11*, 179–246.
- (30) Hayes, R. L.; Noel, J. K.; Mohanty, U.; Whitford, P. C.; Hennelly, S. P.; Onuchic, J. N.; Sanbonmatsu, K. Y. Magnesium fluctuations modulate RNA dynamics in the SAM-I riboswitch. *J. Am. Chem. Soc.* **2012**, *134*, 12043–12053.
- (31) Foloppe, N.; MacKerell, A. D., Jr. All-atom empirical force field for nucleic acids: I. Parameter optimization based on small molecule and condensed phase macromolecular target data. *J. Comput. Chem.* **2000**, *21*, 86–104.
- (32) Denning, E. J.; Priyakumar, U. D.; Nilsson, L.; Mackerell, A. D., Jr. Impact of 2'-hydroxyl sampling on the conformational properties of RNA: update of the CHARMM all-atom additive force field for RNA. J. Comput. Chem. 2011, 32, 1929–1943.
- (33) Aduri, R.; Psciuk, B. T.; Saro, P.; Taniga, H.; Schlegel, H. B.; SantaLucia, J. AMBER Force Field Parameters for the Naturally Occurring Modified Nucleosides in RNA. *J. Chem. Theory Comput.* **2007**, *3*, 1464–1475.
- (34) Chen, A. A.; Garcia, A. E. High-resolution reversible folding of hyperstable RNA tetraloops using molecular dynamics simulations. *Proc. Natl. Acad. Sci. U. S. A.* **2013**, *110*, 16820–16825.
- (35) Pinamonti, G.; Paul, F.; Noé, F.; Rodriguez, A.; Bussi, G. The mechanism of RNA base fraying: Molecular dynamics simulations analyzed with core-set Markov state models. *J. Chem. Phys.* **2019**, *150*, 154123.
- (36) Jasiński, M.; Feig, M.; Trylska, J. Improved Force Fields for Peptide Nucleic Acids with Optimized Backbone Torsion Parameters. *J. Chem. Theory Comput.* **2018**, *14*, 3603–3620.
- (37) Debye, P.; Huckel, E. The theory of electrolytes I. The lowering of the freezing point and related occurrences. *Phys. Z* **1923**, 24, 185–206
- (38) Debye, P.; Huckel, E. The theory of the electrolyte II The border law for electrical conductivity. *Phys. Z* **1923**, *24*, 305–325.

- (39) Nikzad, S.; Noshad, H.; Motevali, E. Study of nonlinear Poisson-Boltzmann equation for a rodlike macromolecule using the pseudo-spectral method. *Results Phys.* **2017**, *7*, 3938–3945.
- (40) Grochowski, P.; Trylska, J. Continuum molecular electrostatics, salt effects, and counterion binding–a review of the Poisson-Boltzmann theory and its modifications. *Biopolymers* **2008**, *89*, 93–113.
- (41) Hayes, R. L.; Noel, J. K.; Mandic, A.; Whitford, P. C.; Sanbonmatsu, K. Y.; Mohanty, U.; Onuchic, J. N. Generalized Manning Condensation Model Captures the RNA Ion Atmosphere. *Phys. Rev. Lett.* **2015**, *114*, No. 258105.
- (42) Roy, S.; Hennelly, S. P.; Lammert, H.; Onuchic, J. N.; Sanbonmatsu, K. Y. Magnesium controls aptamer-expression platform switching in the SAM-I riboswitch. *Nucleic Acids Res.* **2019**, *47*, 3158–3170.
- (43) Roy, S.; Lammert, H.; Hayes, R. L.; Chen, B.; LeBlanc, R.; Dayie, T. K.; Onuchic, J. N.; Sanbonmatsu, K. Y. A magnesium-induced triplex pre-organizes the SAM-II riboswitch. *PLoS Comput. Biol.* 2017, 13, No. e1005406.
- (44) Lammert, H.; Wang, A. L.; Mohanty, U.; Onuchic, J. N. RNA as a Complex Polymer with Coupled Dynamics of Ions and Water in the Outer Solvation Sphere. *J. Phys. Chem. B* **2018**, *122*, 11218–11227.
- (45) Hayatshahi, H. S.; Roe, D. R.; Galindo-Murillo, R.; Hall, K. B.; Cheatham, T. E., 3rd Computational Assessment of Potassium and Magnesium Ion Binding to a Buried Pocket in GTPase-Associating Center RNA. *J. Phys. Chem. B* **2017**, *121*, 451–462.
- (46) Yamagami, R.; Bingaman, J. L.; Frankel, E. A.; Bevilacqua, P. C. Cellular conditions of weakly chelated magnesium ions strongly promote RNA stability and catalysis. *Nat. Commun.* **2018**, *9*, 2149.
- (47) Roy, S.; Onuchic, J. N.; Sanbonmatsu, K. Y. Cooperation between Magnesium and Metabolite Controls Collapse of the SAM-I Riboswitch. *Biophys. J.* **2017**, *113*, 348–359.
- (48) Lu, C.; Ding, F.; Chowdhury, A.; Pradhan, V.; Tomsic, J.; Holmes, W. M.; Henkin, T. M.; Ke, A. SAM recognition and conformational switching mechanism in the Bacillus subtilis yitJ S box/SAM-I riboswitch. *J. Mol. Biol.* **2010**, *404*, 803–818.
- (49) Montange, R. K.; Mondragón, E.; van Tyne, D.; Garst, A. D.; Ceres, P.; Batey, R. T. Discrimination between closely related cellular metabolites by the SAM-I riboswitch. *J. Mol. Biol.* **2010**, 396, 761–772.
- (50) Wang, J. M.; Cieplak, P.; Kollman, P. A. How well does a restrained electrostatic potential (RESP) model perform in calculating conformational energies of organic and biological molecules? *J. Comput. Chem.* **2000**, *21*, 1049–1074.
- (51) Pérez, A.; Marchán, I.; Svozil, D.; Sponer, J.; Cheatham, T. E., 3rd; Laughton, C. A.; Orozco, M. Refinement of the AMBER force field for nucleic acids: improving the description of alpha/gamma conformers. *Biophys. J.* 2007, 92, 3817–3829.
- (52) Zgarbova, M.; Otyepka, M.; Šponer, J.; Mládek, A.; Banáš, P.; Cheatham, T. E., 3rd; Jurečka, P. Refinement of the Cornell et al. Nucleic Acids Force Field Based on Reference Quantum Chemical Calculations of Glycosidic Torsion Profiles. *J. Chem. Theory Comput.* 2011, 7, 2886–2902.
- (53) Barca, G. M. J.; Bertoni, C.; Carrington, L.; Datta, D.; De Silva, N.; Deustua, J. E.; Fedorov, D. G.; Gour, J. R.; Gunina, A. O.; Guidez, E.; et al. Recent developments in the general atomic and molecular electronic structure system. *J. Chem. Phys.* **2020**, *152*, 154102.
- (54) Dupradeau, F. Y.; Pigache, A.; Zaffran, T.; Savineau, C.; Lelong, R.; Grivel, N.; Lelong, D.; Rosanski, W.; Cieplak, P. The R.E.D. tools: advances in RESP and ESP charge derivation and force field library building. *Phys. Chem. Chem. Phys.* **2010**, *12*, 7821–7839.
- (55) Cornell, D. W. C. P.; Cieplak, P.; Bayly, C. I.; Kollman, P. A. Application of RESP charges to calculate conformational energies, hydrogen bond energies, and free energies of solvation. *J. Am. Chem. Soc.* 1993, 115, 9620–9631.
- (56) Wang, J.; Wolf, R. M.; Caldwell, J. W.; Kollman, P. A.; Case, D. A. Development and testing of a general amber force field. *J. Comput. Chem.* **2004**, *25*, 1157–1174.

- (57) Dang, L. X. Mechanism and Thermodynamics of Ion Selectivity in Aqueous-Solutions of 18-Crown-6 Ether a Molecular-Dynamics Study. J. Am. Chem. Soc. 1995, 117, 6954–6960.
- (58) Bai, Y.; Greenfeld, M.; Travers, K. J.; Chu, V. B.; Lipfert, J.; Doniach, S.; Herschlag, D. Quantitative and comprehensive decomposition of the ion atmosphere around nucleic acids. *J. Am. Chem. Soc.* **2007**, *129*, 14981–14988.
- (59) Aqvist, J. Ion-water interaction potentials derived from free energy perturbation simulations. *J. Phys. Chem.* **1990**, *94*, 8021–8024.
- (60) Stoddard, C. D.; Montange, R. K.; Hennelly, S. P.; Rambo, R. P.; Sanbonmatsu, K. Y.; Batey, R. T. Free state conformational sampling of the SAM-I riboswitch aptamer domain. *Structure* **2010**, 18, 787–797.
- (61) McDaniel, B. A.; Grundy, F. J.; Henkin, T. M. A tertiary structural element in S box leader RNAs is required for S-adenosylmethionine-directed transcription termination. *Mol. Microbiol.* **2005**, *57*, 1008–1021.
- (62) Schroeder, K. T.; Daldrop, P.; Lilley, D. M. J. RNA tertiary interactions in a riboswitch stabilize the structure of a kink turn. *Structure* **2011**, *19*, 1233–1240.